AD-A147 433 PHOTOCHEMISTRY AND KINETICS OF THE O*2-HI SYSTEM(U) 1/1
AEROSPACE CORP EL SEGUNDO CA AEROPHYSICS LAB
J B KOFFEND ET AL. 10 SEP 84 TR-0084(4610)-1
UNCLASSIFIED SD-TR-84-37 F04701-83-C-0084 F/G 20/5 NL

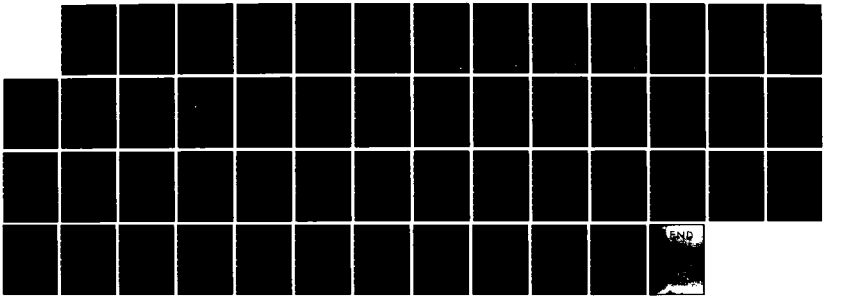

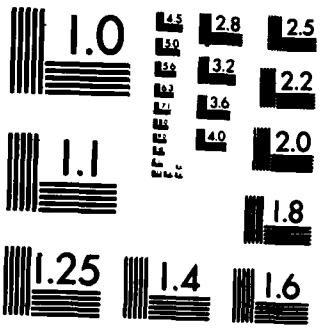
1.0
1.1
1.25
1.4
1.6
1.8
2.0
2.2
2.5
2.8
3.2
3.6
4.0
4.5
5.0
5.6

REPORT SD-TR-84-37

(12)

Photochemistry and Kinetics of the O_2^*-HI System

J. B. KOFFEND, C. E. GARDNER,
and R. F. HEIDNER III
Aerophysics Laboratory
Laboratory Operations
The Aerospace Corporation
El Segundo, Calif. 90245

O_2^*

10 September 1984

Prepared for

SPACE DIVISION
AIR FORCE SYSTEMS COMMAND
Los Angeles Air Force Station
P.O. Box 92960, Worldway Postal Center
Los Angeles, Calif. 90009

A

This report was submitted by The Aerospace Corporation, El Segundo, CA 90245, under Contract No. F04701-82-C-0083 with the Space Division, P.O. Box 92960, Worldway Postal Center, Los Angeles, CA 90009. It was reviewed and approved for The Aerospace Corporation by W. P. Thompson, Director, Aerophysics Laboratory. Captain Douglas H. Olsen, SD/YNS, was the project officer for the Mission Oriented Investigation and Experimentation (MOIE) Program.

This report has been reviewed by the Public Affairs Office (PAS) and is releasable to the National Technical Information Service (NTIS). At NTIS, it will be available to the general public, including foreign nationals.

This technical report has been reviewed and is approved for publication. Publication of this report does not constitute Air Force approval of the report's findings or conclusions. It is published only for the exchange and stimulation of ideas.

Capt. Douglas H. Olsen
SD/YNS
Laser Effects Project Officer

Joseph Hess, GM-15, Director
West Coast Office
AF Space Technology Center

UNCLASSIFIED

SECURITY CLASSIFICATION OF THIS PAGE (When Data Entered)

REPORT DOCUMENTATION PAGE	READ INSTRUCTIONS BEFORE COMPLETING FORM
1. REPORT NUMBER: SD-TR-84-37	2. GOVT ACCESSION NO.: A147433
3. RECIPIENT'S CATALOG NUMBER:	
4. TITLE (and Subtitle): PHOTOCHEMISTRY AND KINETICS OF THE O_2^*-HI SYSTEM	5. TYPE OF REPORT & PERIOD COVERED:
6. PERFORMING ORG. REPORT NUMBER: TR-0084(4610)-1	
7. AUTHOR(s): J. B. Koffend, C. E. Gardner, and R. F. Heidner III	8. CONTRACT OR GRANT NUMBER(s): F04701-83-C-0084
9. PERFORMING ORGANIZATION NAME AND ADDRESS: The Aerospace Corporation, El Segundo, Calif. 90245	10. PROGRAM ELEMENT, PROJECT, TASK AREA & WORK UNIT NUMBERS:
11. CONTROLLING OFFICE NAME AND ADDRESS: Space Division, Los Angeles Air Force Station, Los Angeles, California 90009	12. REPORT DATE: 10 September 1984
	13. NUMBER OF PAGES: 42
14. MONITORING AGENCY NAME & ADDRESS (if different from Controlling Office)	15. SECURITY CLASS. (of this report): Unclassified
	15a. DECLASSIFICATION/DOWNGRADING SCHEDULE:

16. DISTRIBUTION STATEMENT (of this Report)

Approved for public release; distribution unlimited.

17. DISTRIBUTION STATEMENT (of the abstract entered in Block 20, if different from Report)

18. SUPPLEMENTARY NOTES

less than dX10 to the minus 17th power CC

Superscript 3P Subscript 1/2 10 to the minus 14th power CC

19. KEY WORDS (Continue on reverse side if necessary and identify by block number)

Chemical kinetics
Chemical lasers
Electronically-excited oxygen
Energy transfer
Iodine atoms
Photochemistry + or -

Superscript 1 Delta Superscript 1 Sigma

20. ABSTRACT (Continue on reverse side if necessary and identify by block number)

Rate coefficients of 42 × 10^{-17} cm^3/molecule-sec and (2.7 ±1.0) × 10^{-14} cm^3/molecule-sec have been measured by flow tube techniques for HI quenching of $O_2(^1\Delta)$ and $O_2(^1\Sigma)$, respectively. In a separate experiment, the quantum yields of $I(^2P_{1/2})$ from HI and CF_3I photolysis at 249 nm were determined to be (0.65 ± 0.04) and (0.88 ± 0.06), respectively, relative to a quantum yield of 1.0 from the photolysis of n-C_3F_7I. The quenching rate of

Cont'd

DD FORM 1473 (FACSIMILE) + or -

UNCLASSIFIED

SECURITY CLASSIFICATION OF THIS PAGE (When Data Entered)

19. KEY WORDS (Continued)

10 to the Minus 14th powers

+ or -

20. ABSTRACT (Continued)

I^* by HI was determined to be $(5.7 \pm 1.0) \times 10^{-14}$ cm^3/molecule-sec. Experimental data and modeling results are presented for photolysis of a mixture of O_2^* and HI. These data are relevant to consideration of a pulsed version of the chemical oxygen-iodine laser (COIL).

PREFACE

The authors would like to acknowledge the help of Dr. R. Hofland and Dr. J. F. Bott on modeling problems associated with this system. Dr. J. A. Betts kindly provided a copy of Ref. 26. We thank W. Hansen, J. Rodriguez, G. I. Segal, and Dr. J. V. V. Kasper for assistance in developing the experimental apparatus and data acquisition system.

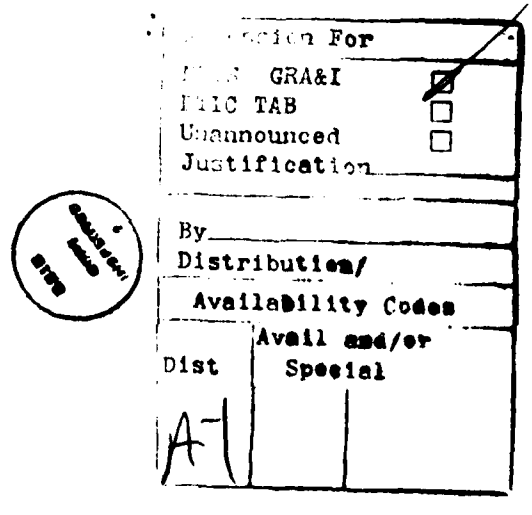

CONTENTS

FIGURES

TABLES

I. INTRODUCTION

There has been intense recent interest in the study of the chemically pumped oxygen-iodine laser (COIL).[1-3] The purpose of this report is to examine the photochemistry and kinetics of a hybrid version of COIL, which operates in a pulsed (or repetitively pulsed) mode rather than as a continuous-wave device. A search was conducted to identify a photolytic I-atom precursor that is stable in O_2^* and that is an inefficient deactivator of $O_2(^1\Delta)$, $O_2(^1\Sigma)$, and I^*. A pulsed oxygen-iodine laser would have properties substantially different from the well-known photolytic I^* laser that has been the subject of extensive review articles.[4,5] In a COIL device, each I atom is pumped from the $I(^2P_{3/2})$ ground state to the $I(^2P_{1/2})$ excited state many times by the excited oxygen. Since the O_2^* is in great excess over the I atoms ($\sim$ 100 to 1), the energetic efficiency of the initial I atom production is the primary measure of overall laser performance. I_2 is the source of I atoms in a conventional COIL device and has been considered as a source of I atoms for a pulsed version of COIL.[6,7] In both cases, complex energy transfer processes result in an O_2^*-driven chain reaction mechanism for I_2 dissociation.[8,9] The $O_2(^1\Delta)$ consumed in this dissociation process represents lost output laser power on the I atom transition; however, there may be a more serious limitation on laser performance. In many instances, the I_2 dissociation process outruns O_2^*-I_2 mixing by laminar diffusion. The resulting gain medium is spatially inhomogeneous, which adversely affects the optical quality of the output laser beam.

An obvious second choice for an I-atom precursor in a premixed, photolytically initiated COIL system would be one of the perfluoroalkyl iodides. These compounds give extremely high I^* quantum yields upon photolysis in the near ultraviolet.[5] Although $O_2(^1\Delta)$ quenching by most atoms and molecules is extremely slow, many perfluoroalkyl iodides react rapidly with O_2^* in a highly complex manner.[10,11] We will demonstrate in this report that this undesirable behavior is not observed when HI is used as the I-atom precursor. We have determined rate coefficients for $O_2(^1\Delta$ and $^1\Sigma)$ quenching by HI in a computer-

controlled flow tube apparatus that has been extensively described in earlier publications.[8,12,13] The measured quenching rates are sufficiently small to permit premixing HI ([HI] > $10^{16}/cm^3$) with O_2^* for time periods approaching 1 sec. Thus, one can obtain a high degree of medium homogeneity prior to photoinitiation.

In order to test the pulsed production of I atoms in O_2^* in the cleanest possible manner, we photolyzed HI with a KrF laser at λ = 249 nm. The quantum yield of I^* from the HI photolysis was measured relative to that from n-C_3F_7I in Ar buffer gas. The CF_3I quantum yield was also measured for comparison. The time behavior of I^* created by the photolysis of HI can be complex, as earlier work using broadband flash photolysis has shown. The secondary reactions possible in the HI/Ar system are discussed. Subsequently, the time behavior of I^* and $O_2(^1\Sigma)$ was measured under identical conditions of HI photolysis with the Ar buffer replaced by a stream of electronically excited oxygen. Modeling calculations are discussed that evaluate these results for the low $^1\Delta/^3\Sigma$ ratios produced by discharge methods and that enable us to predict kinetic behavior at $O_2(^1\Delta)$ levels attainable with a chemical generator of excited oxygen.[1-3]

II. EXPERIMENTAL APPARATUS AND PROCEDURES

A. COMPUTER-CONTROLLED FLOW TUBE APPARATUS

This apparatus has been described extensively in earlier publications.[8,12,13] Electronically excited oxygen is created by a microwave discharge in pure oxygen. The O atoms produced by the discharge are removed on a heated HgO ring formed on the inside of the discharge tube by co-discharging O_2 and Hg prior to experimentation. The density of $O_2(^1\Delta)$ is determined by isothermal calorimetry following the procedure of Trainor et al.[14] All other flow rates (O_2, Ar, and HI) are measured with Tylan digital flowmeters or by Matheson rotamers calibrated by pressure rise measurements in a known volume and cross calibrated against the digital flowmeters. Pressure is measured by an MKS TruTorr capacitance manometer. All flow and pressure data are entered into a PDP 11/10 computer that evaluates the partial pressures and flow parameters of the experiment in real time.

The densities of $O_2(^1\Delta)$, $O_2(^1\Sigma)$, and I^* are monitored by emission spectroscopy in the visible and near infrared. Two spectrometer systems are mounted on a platform whose movement is regulated by a computer-controlled stepping motor. At discrete positions along the flow tube (typically 50), the computer samples the signal from both the visible emission channel (1/4-m monochromator, GaAs phototube, and photon counter) and the near infrared emission channel (1/4-m monochromator, intrinsic Ge detector, and lock-in amplifier).

The flow tube was constructed of Pyrex tubing 3.8 cm i.d. with a 60-cm usable length. It was internally coated with halocarbon wax to inhibit the wall recombination of any iodine atoms formed. In addition, halocarbon wax forms an extremely inert surface for deactivation of electronically excited O_2. The gases used in this apparatus were O_2 (Matheson, 99.99%), Ar (Matheson, 99.9995%), and HI (Matheson, 98%). The O_2 and Ar were passed at atmospheric pressure through Linde 5A molecular sieve traps which had been baked at 200°C under vacuum prior to experimentation. HI was purified by a series of trap-to-trap distillations from 230 to 77 K. When HI was introduced

into the system, it flowed through a Pyrex-wool-packed trap held at 195 K. Despite these precautions, there is evidence that some I_2 does reach the O_2^* flow, which results in a low level production of I atoms (see Section III). An alternative explanation is that trace $O(^3P)$ atoms bypass the HgO ring and react with the added HI to form the I atoms.

B. EXCIMER LASER PHOTOLYSIS APPARATUS

The excimer laser photolysis apparatus is shown schematically in Fig. 1. The gas handling system is virtually identical to that described above. The mixture of HI, O_2, and Ar was slowly flowed through a quartz cell 4.5 cm i.d. and 60 cm long to minimize the deactivation of $O_2(^1\Delta)$ by HI and replace the gas mixture between laser shots. The Lambda Physik EMG 101 excimer laser was operated with stable cavity optics at 249 nm with repetition rates of 1 to 10 Hz. The 1 × 2.8 cm unfocused beam had an energy of < 200 mJ/pulse resulting in an illumination intensity of < 5 MW/cm^2. Suprasil quartz windows both normal to and at Brewster's angle to the laser radiation were tested. The normal incidence windows were used in the experiments reported here. I^* and $O_2(^1\Delta)$ emissions (λ = 1.315 and 1.27 μm, respectively) were detected by means of a high-speed intrinsic Ge detector viewing through narrow band interference filters (10 nm FWHM). $O_2(^1\Sigma)$ was detected by a cooled GaAs photomultiplier-interference filter combination at λ = 7619 A. Laser energy was measured with a Scientech 4 in. diameter calorimeter. Gross attenuation of the KrF beam (factors of 10 to 100) was accomplished by using a quartz flat in positions S1 and/or S2 of the four-element optical path shown in Fig. 1. Finer attenuation (a factor of 3 or less) was achieved by inserting a stack of quartz plates into the optical path. The Tylan flowmeters were recalibrated under our exact experimental conditions for all the gases used in this study by pressure rise versus time measurements in the same calibrated volume. All such curves were precisely linear over the flow ranges employed.

The transient signals from the laser photolysis were digitized on a Biomation 805 transient recorder and summed in a Nicolet 1072 signal averager. Up to 128 traces were summed and transferred to a DEC LSI 11/23 minicomputer for storage and analysis.

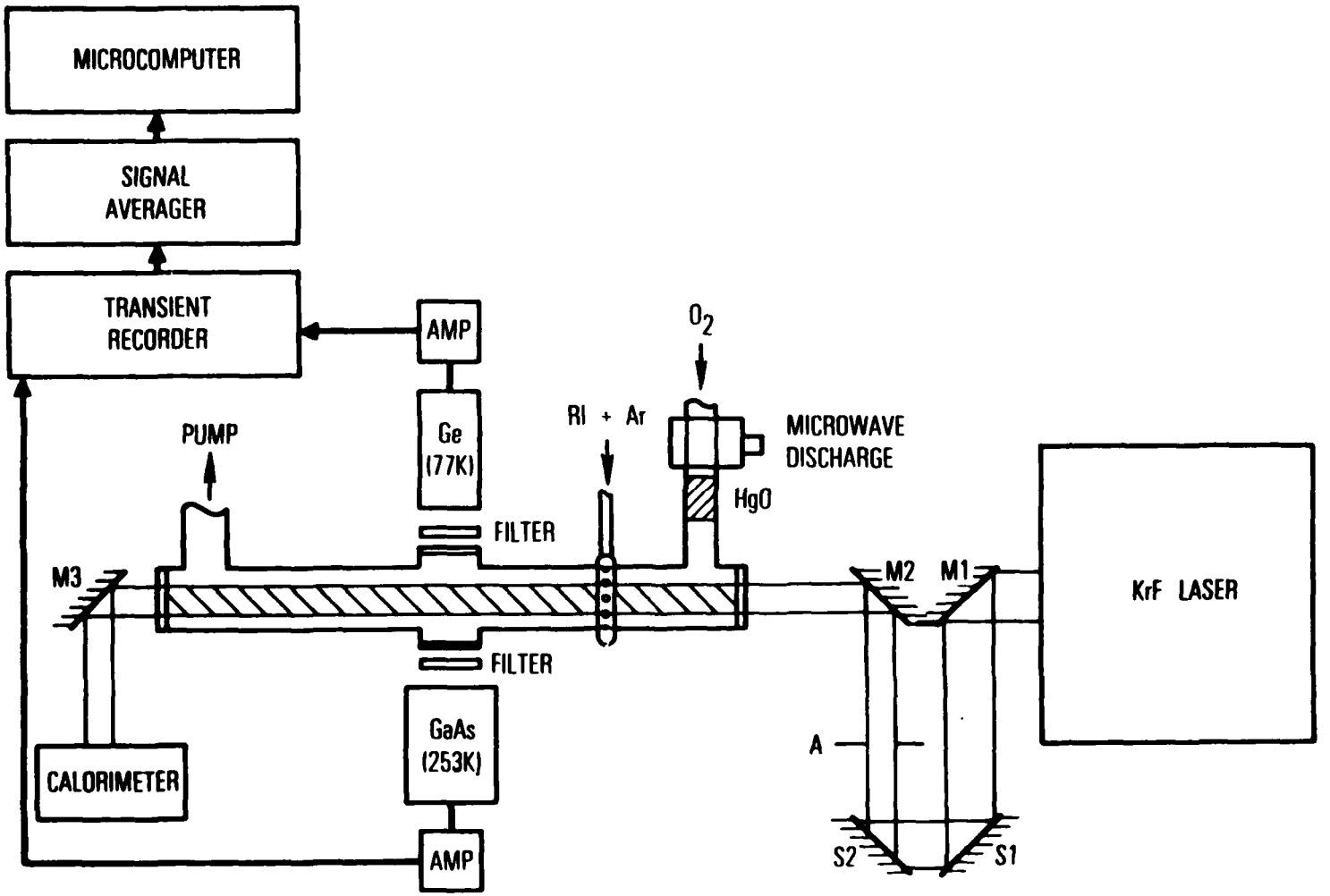

Fig. 1. Excimer laser photolysis apparatus.

III. RESULTS AND ANALYSIS

A. KINETIC FLOW TUBE

The rate coefficient for $O_2(^1\Delta)$ removal by HI has been measured by monitoring the decay of 1.27-μm emission along the flow tube following injection of HI (Fig. 2):

$$O_2(^1\Delta) + HI \overset{k_1}{\rightarrow} O_2(^3\Sigma) + HI \qquad (1)$$

Some I^* appears rapidly in the flow tube at short times. The I atoms are attributed either to O_2^*-driven dissociation of I_2 impurity in the HI or to the reaction of trace $O(^3P)$ atoms (those not recombined on the HgO surface) with HI. Pirkle et al.[15] used Reaction (2)

$$O(^3P) + HI \overset{k_{2a}}{\rightarrow} OH + I^* \qquad (2a)$$

$$\overset{k_{2b}}{\rightarrow} OH + I \qquad (2b)$$

in an attempt to produce a cw I-atom laser. They injected HI into a system of discharged O_2 containing both $O(^3P)$ and O_2^*. I^* is produced by Reaction (2a) and by the fast equilibrium[16,17]

$$O_2(^1\Delta) + I \underset{k_{-3}}{\overset{k_3}{\rightleftarrows}} O_2(^3\Sigma) + I^* \qquad (3)$$

$$K_{eq} = k_3/k_{-3} = 2.9 \ (T = 295 \ K)$$

The rapid decay of I^* observed in Ref. 15 is most probably associated with the creation of substantial amounts of H_2O. The analysis of these data will be discussed in Section IV. The HgO surface recombination of $O(^3P)$ in the present kinetic flow tube apparatus eliminates any quenching of the coupled I^*-$O_2(^1\Delta)$ states (Fig. 2) upon HI addition that cannot be explained by the process

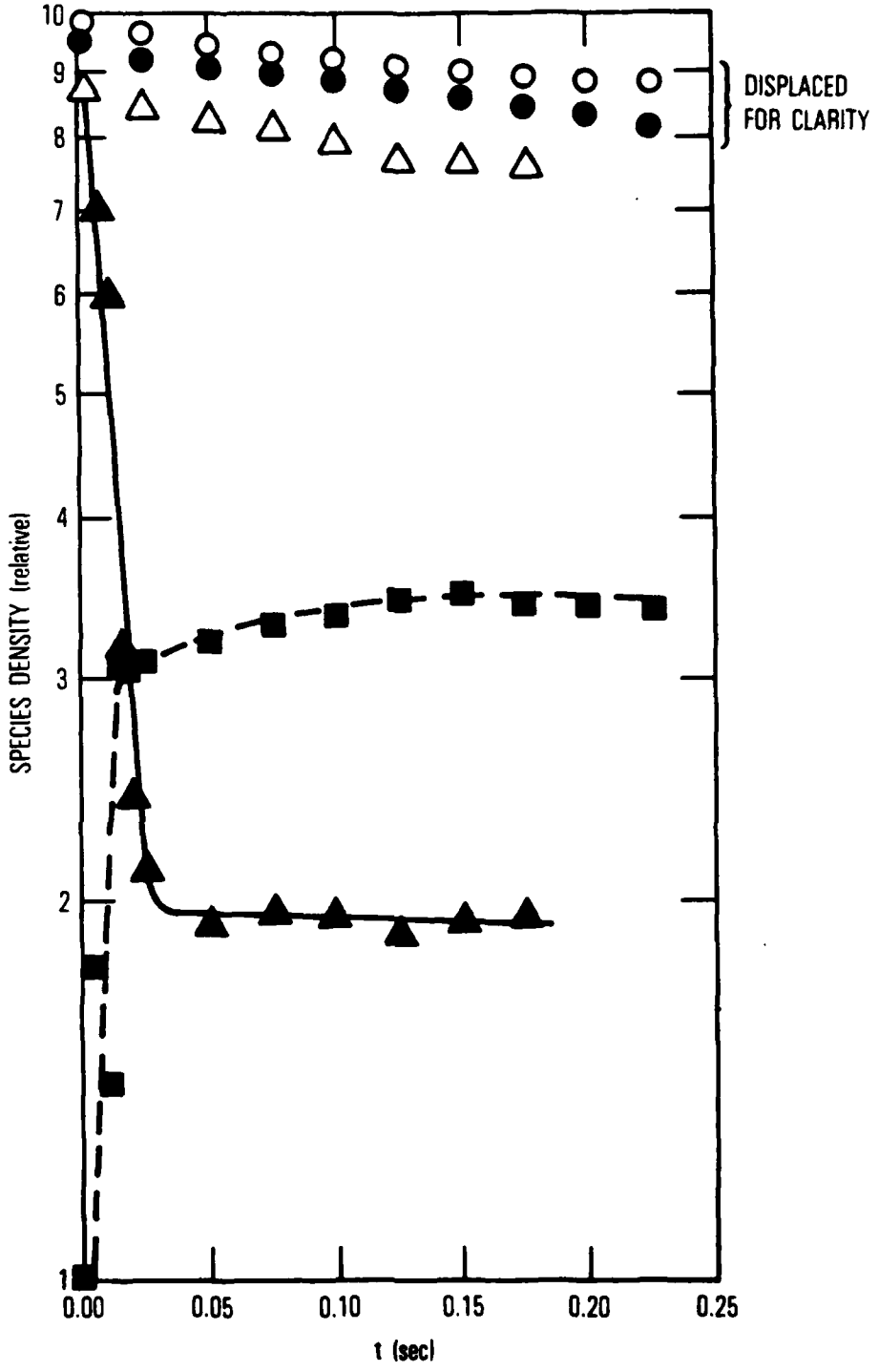

Fig. 2. O_2^* deactivation by HI. Conditions: P = 3.14 Torr, $[^1\Delta]_0 = 5 \times 10^{15}$, $[I^*]_{max} = 3 \times 10^{11}$, $[I]_{max} = 7 \times 10^{11}/cm^3$.
[HI] = 0: $O_2(^1\Delta)$ -○, $O_2(^1\Sigma)$ -△
[HI] = $6 \times 10^{15}/cm^3$: $O_2(^1\Delta)$ -●, $O_2(^1\Sigma)$ -▲, I^* -■.

$$O_2(^1\Delta) + I^* \xrightarrow{k_{4a}} O_2(^1\Sigma) + I \qquad (4a)$$

$$\xrightarrow{k_{4b}} \text{Other Products} \qquad (4b)$$

Previous work in our laboratory has found $k_{4a} = 1.1 \times 10^{-13}$ cm^3/molecule-sec.[12] Further work in progress has yielded an estimate of $k_4 = 2 \times 10^{-13}$ cm^3/molecule-sec.[18] On the basis of the current data and previous results, we find $k_1 < 2 \times 10^{-17}$ cm^3/molecule-sec.

The quenching of $O_2(^1\Sigma)$ by HI is significantly easier to study. $O_2(^1\Sigma)$ is constantly being produced by the energy pooling Processes (4a) and (5)

$$O_2(^1\Delta) + O_2(^1\Delta) \xrightarrow{k_5} O_2(^1\Sigma) + O_2(^3\Sigma) \qquad (5)$$

and removed by

$$O_2(^1\Sigma) + HI \xrightarrow{k_6} O_2(^3\Sigma) + HI \qquad (6)$$

as well as by wall collisions and gas-phase collisions with buffer gas and impurity species. The quenching of $O_2(^1\Sigma)$ by HI can be determined either by a time-resolved approach to steady state[12,19] or by Stern-Volmer analysis in steady state. We have relied on the former method to measure the absolute rate (sec^{-1}) of $O_2(^1\Sigma)$ quenching in the absence of HI

$$[^1\Sigma] = [^1\Sigma]_{ss} \exp(-2k_\Delta^0 t) - \{[^1\Sigma]_{ss} - [^1\Sigma]_0\} \exp(-k_\Sigma^0 t) \qquad (7)$$

A value $(k_\Sigma^0) = (25 \pm 5)$ sec^{-1} was determined from Eq. (7) by the method described in Ref. 12, where k_Σ^0 and k_Δ^0 represent wall and background gas phase (typically H_2O) quenching of $O_2(^1\Sigma)$ and $O_2(^1\Delta)$, respectively. $[^1\Sigma]_0$ and $[^1\Sigma]_{ss}$ are the initial and steady-state densities of $O_2(^1\Sigma)$, respectively. If mixing is rapid with respect to the kinetic time scales, it is possible to analyze the time-resolved approach to a new $O_2(^1\Sigma)$ steady state

caused by the introduction of HI (see Fig. 2 and Ref. 12) in order to determine k_6. This method was not used in the present study. Instead, we have used the Stern-Volmer relationship, i.e., the ratio of steady-state $O_2(^1\Sigma)$ densities with and without added HI to determine k_6 ($[O_2(^1\Delta)]$ is constant)

$$\frac{I_\Sigma^0}{I_\Sigma}\left\{1 + \frac{k_{4a}[I^*]}{k_5[^1\Delta]}\right\} - 1 = \frac{k_6}{k_\Sigma^0}[HI] \qquad (8)$$

where I_Σ and I_Σ^0 are the emission intensities of the $O_2(^1\Sigma)$ band at 762 nm in the presence and absence of HI, respectively. The second bracket on the left-hand side of Eq. (8) contains a small correction for incremental $O_2(^1\Sigma)$ pumping $k_{4a}[I^*]/k_5[^1\Delta]$ created by addition of the HI. A value $k_6 = (2.5 \pm 1.0) \times 10^{-14}$ cm^3/molecule-sec was determined from $O_2(^1\Sigma)$ data such as those shown in Fig. 2 by plotting the left-hand side of Eq. (8) versus [HI] and multiplying the slope by the value of k_Σ^0 determined from Eq. (7).

B. PHOTOCHEMISTRY OF HI, CF_3I, AND C_3F_7I AT λ = 249 nm

The subject of iodide photolysis in relation to the I^* laser has been reviewed recently.[5,20] HI photolysis has been extensively studied as a source of translationally excited H atoms.[21-23]

$$HI + h\nu \rightarrow H + I(^2P_{1/2}) \qquad (9a)$$

$$\rightarrow H + I(^2P_{3/2}) \qquad (9b)$$

Mulliken[24] predicted that the observed ultraviolet continuum is a convolution of three separate transitions: a parallel $^1\Sigma \rightarrow {}^3\pi_0{}^+$ transition resulting in $I(^2P_{1/2})$ production and two perpendicular transitions ($^1\Sigma \rightarrow {}^3\pi$ and $^1\pi$) yielding $I(^2P_{3/2})$. There is ample evidence to support his assignment of the $^1\Sigma \rightarrow {}^3\pi_0{}^+$ transition to the region of the absorption maximum. Qualitatively, I^* quantum yields show such a maximum for both HI[25] and DI[26] photolysis. In addition, Clear et al.[25] demonstrated by photofragment spectroscopy that 266.2 nm photolysis yields products from perpendicular (67%) and from parallel (33%) transitions. Confirmation of this result has come from an elegant recent study of HI photolysis by tunable VUV laser spectroscopy of the Lyman-α transition.[23]

Quantum yields for both $I(^2P_{1/2})$ and $I(^2P_{3/2})$ have been determined for a number of alkyl iodides and for HI using atomic absorption spectroscopy.[27,28] Continuum flash photolysis was used in these experiments and, therefore, the reported quantum yields are averaged over the absorption band of the precursor and the energy spectrum of the flashlamp. A frequently used technique for I^* quantum yields involves monitoring the I^* emission at $\lambda = 1.315$ μm from a "standard" and an "unknown" precursor in the same photolysis geometry. This technique can be used in order to obtain relative I^* quantum yields or the wavelength or temperature dependence of quantum yield. Recent work has shown such measurements to be complicated by the presence of exciplex (i.e., excited complex) emission at wavelengths slightly shifted from the I^* transition[29-31]

$$I^* + M \underset{k_{-10a}}{\overset{k_{10a}}{\rightleftarrows}} I^*M \qquad (10a)$$

$$I^*M \xrightarrow{k_{10b}} I + M + h\nu_{ex} \qquad (10b)$$

where M is the iodine atom precursor or the buffer gas. Early quantum yield work using this method for HgI_2,[32] CH_2I_2,[33] and perfluoroalkyl iodides has been slightly modified and extended by Smedley and Leone[31] to account for this exciplex emission in a quantitative fashion.

We have employed this method to measure the I^* quantum yield from CF_3I and HI in a density regime of I-atom precursor (< 0.3 Torr) and buffer gas (< 5 Torr) where corrections for exciplex emission are not necessary.[29] Exciplex emission involving HI as a precursor has not been reported, but must be negligible under these experimental conditions. The obvious choice for a standard precursor is $n\text{-}C_3F_7I$ where the absorption-band-averaged I^* quantum yield is > 99%[28], and no measurable wavelength dependence is exhibited between 265 and 298 nm.[31] We have assumed in this work that the I^* quantum yield is 1.0 at $\lambda = 249$ nm. The quantum yield of I^* from photolyzing an unknown precursor can be computed as follows:

$$\frac{Q_{RI}}{Q_S} = \frac{[I^*]_{RI}(t=0)}{[I^*]_S(t=0)} \cdot \frac{P_S}{P_{RI}} \cdot \frac{W_S}{W_{RI}} \cdot \frac{\sigma_S}{\sigma_{RI}} \qquad (11)$$

where RI indicates the unknown precursor iodide (HI or CF_3I); S is the quantum yield standard ($n\text{-}C_3F_7I$); and Q, P, W, and σ are the I^* quantum yield, precursor pressure, laser flux, and absorption cross section of the precursor at λ = 249 nm, respectively. Thus, the quantum yield ratio is computed from the four measured ratios defined on the right-hand side of Eq. (11). This methodology removes most of the systematic errors inherent in the experiment. To evaluate the precursor pressures precisely, the digital flowmeters were calibrated as described earlier. The partial pressure of each gas was calculated from the ratio of its molar flow to the total flow multiplied by the total system pressure. The ultraviolet absorption coefficients for the three I atom precursors were remeasured (Fig. 3 and Table I). Selected data points from Ref. 31 for $n\text{-}C_3F_7I$ and from Ref. 35 for HI are shown for comparison with the present results.

The yield of I^* at t = 0 should be well defined for CF_3I and $n\text{-}C_3F_7I$ precursors. During the photolysis of HI, however, secondary processes can produce I^*. This complication is discussed in this section. As shown in Fig. 4, a fraction of the data is taken on the fastest time scale permitted by our apparatus (200 ns/point). We have no indication from these data that our extrapolation to t = 0 is affected by secondary processes. The experimental data required to analyze Eq. (11) are presented in Table II. The quoted errors represent one standard deviation and are consistent with a propagation of the random errors inherent in the measured quantities in Eq. (11). The quantum yield results are summarized in Table III. As predicted by Mulliken,[24] there is a region of the HI absorption continuum where the $^1\Sigma \rightarrow {}^3\pi_0$+ component of the transition produces a substantial quantum yield of I^*. The deconvolution of the spectrum attempted by Clear et al.[25] is consistent with the present results. Results for DI indicate the same quantum yield peaking in the 240 to 250 nm range.[26] The apparent agreement of the present results with those reported by Cadman and Polanyi[37] must be qualified because these authors employed an I^* Einstein coefficient of 22 sec^{-1} to analyze their data. The value A = 7.8 sec^{-1} has extensive theoretical and experimental justification.[5] Our CF_3I experiments give a quantum yield larger than that reported by Gerck[36] at the same wavelength. The present result is in better

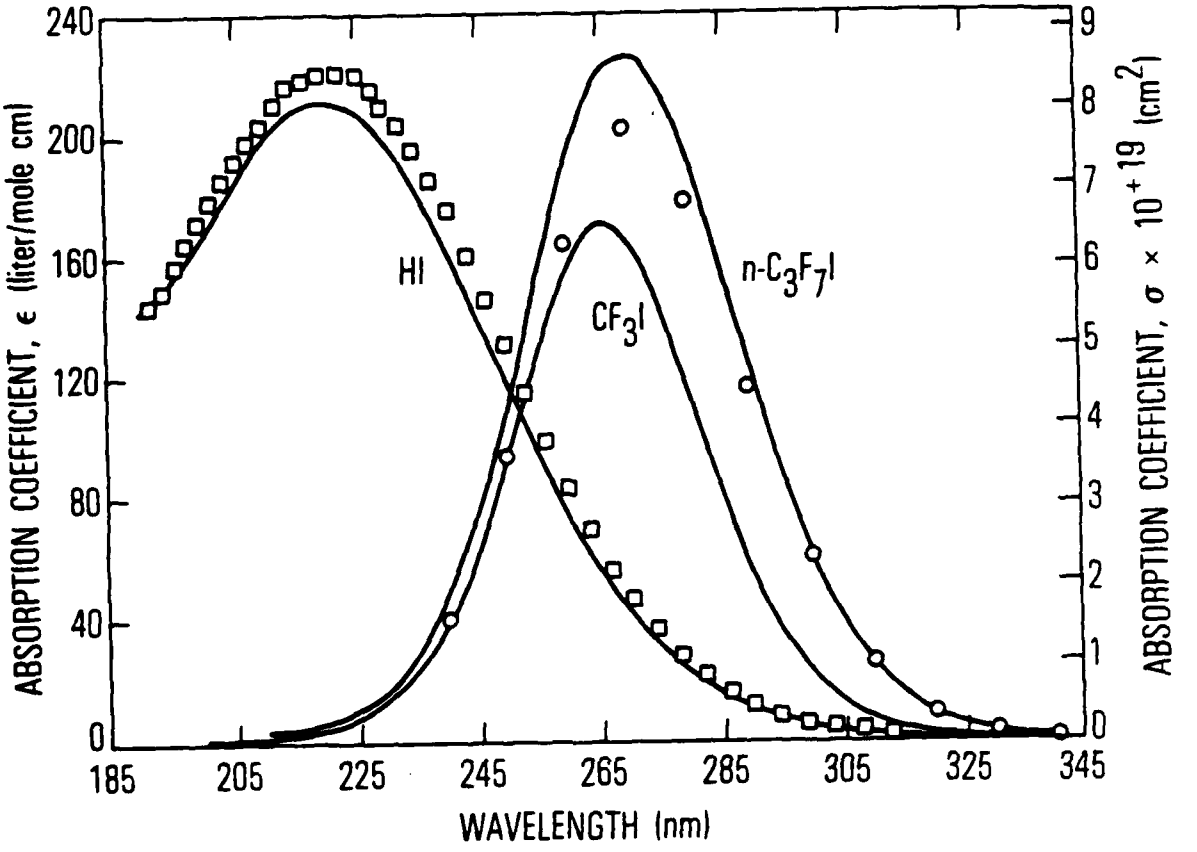

Fig. 3. Ultraviolet absorption cross sections for HI, CF_3I, and n-C_3F_7I. Data points (O) from Ref. 31 and (□) from Ref. 35.

Table I. Ultraviolet Absorption Cross Sections for HI, CF_3I, and $n\text{-}C_3F_7I$

Species	$\sigma(cm^2) \times 10^{+19}$		Reference
	$\sigma_{249\ nm}$	σ_{max}	
HI	4.8	8.1	This Work[a-c]
	5.3	8.4	35
CF_3I	3.2	6.5	This Work
		7.0	34
$n\text{-}C_3F_7I$	3.7	8.6	This Work
		7.7	31
		9.5	34

[a]Cell path length: L = 9.9 cm
[b]Pressure of absorber: 10.0 Torr (MKS Baratron)
[c]Spectra recorded with Beckman 5240 spectrophotometer

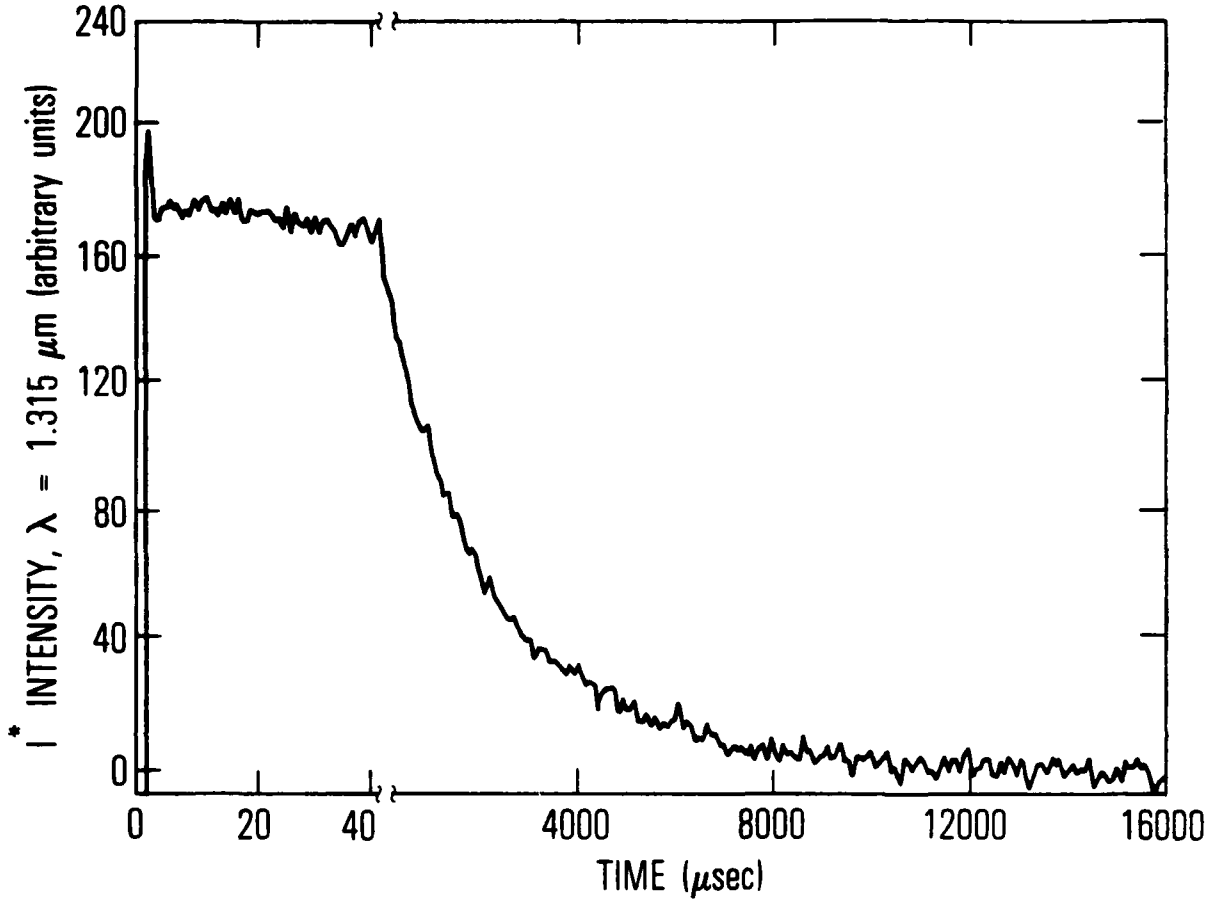

Fig. 4. I^* decay profile from HI photolysis at λ = 248.5 nm.

Table II. I^* Production Data for HI, CF_3I, and $n\text{-}C_3F_7I$ Photolytic Precursors

Species	[RI] ($10^{14}/cm^3$)	$([I^*]+[I]_0$[a] ($10^{12}/cm^3$)	Q[b] (arb)
CF_3I	5.5	5.1	0.85
	8.7	16.3	0.89
	9.0	6.8	0.90
	11.7	10.0	0.93
	15.2	13.9	0.85
	16.6	31.8	0.87

			Q_{av} = 0.88±0.06
HI	9.4	16.7	0.66
	9.5	7.3	0.61
	11.6	16.0	0.69
	14.2	27.3	0.67
	17.4	23.9	0.65
	17.8	30.0	0.70
	17.9	46.1	0.65
	18.0	13.7	0.66
	27.2	38.5	0.62
	31.3	41.3	0.65
	31.9	23.7	0.64
	99.7	250.0	0.66

			Q_{av} = 0.65±0.04
$n\text{-}C_3F_7I$	5.9	9.3	0.997
	10.4	16.2	1.006
	14.3	22.4	0.990
	20.1	31.7	1.008

			Q_{av} = 1.00±0.01

[a]Calculated from [RI], σ, and W.

[b]$Q = ([I^*]/([I^*]+[I])$ was normalized to Q = 1.0 for the mean of the $n\text{-}C_3F_7I$ results.

Table III. Quantum Yield of I^* From Photolysis of HI, CF_3I, and $n\text{-}C_3F_7I$

Species	Wavelength (nm)	Q_I^*	Reference
HI	248.5	0.65±0.04	This Work
	253.7	0.55±0.25[a]	37
	253.7	0.55-0.65	38
	266.2	0.36±0.05	25
	266.2	0.40±0.05	23
	Broadband UV	0.10±0.05	28
DI	214	0.33±0.10	26
	240	0.60±0.07	26
	253.7	0.46±0.05	26
	266.2	0.26±0.03	25
	280	- 0.08±0.27	26
CF_3I	248.5	0.88±0.06	This Work
	248.5	0.75±0.05	36
	308	0.83	36
	Broadband UV	0.90±0.04	27
	Broadband UV	0.91±0.03	28
$n\text{-}C_3F_7I$	248.5	(=1.0)[b]	This Work
	265-298	Constant[b]	31
	Broadband UV	>0.99	28

[a]Derivation of this number assumes an I^* Einstein coefficient of 22 sec^{-1} (see text).
[b]The quantum yield of I^* from $n\text{-}C_3F_7I$ is assumed to be unity.

agreement with measurements employing broadband flash photolysis;[27,28] however, more data as a function of wavelength are necessary to evaluate the quantum yield results of 249 nm.

This general experimental arrangement is suitable for measuring the quenching of I^* by parent compounds and photolysis products. The rate coefficients for I^* quenching by CF_3I and $n\text{-}C_3F_7I$[29] are too small to measure under our experimental conditions. The quenching of I^* by HI is observable; however

$$I^* + HI \xrightarrow{k_{12}} I + HI \tag{12}$$

the kinetic traces can be complex because of the following side reactions:

$$H + HI \xrightarrow{k_{13a}} H_2 + I^* \tag{13a}$$

$$\xrightarrow{k_{13b}} H_2(v) + I \tag{13b}$$

$$I^* + H \xrightarrow{k_{14}} I + H \tag{14}$$

$$I + H_2(v) \underset{k_{-15}}{\overset{k_{15}}{\rightleftarrows}} I^* + H_2(v-2) \tag{15}$$

where $H_2(v)$ indicates the possibility of vibrational excitation ($v < 3$). The total rate for Reaction (13) has been measured to be 2 to 3 $\times 10^{-11}$ cm^3/molecule-sec.[39,40] There is good qualitative evidence that the branching ratio to form I^* (k_{13a}/k_{13}) is small,[37] although the production of I^* from secondary processes (i.e., k_{15}) is significant. Donohue and Wiesenfeld[40] were successful in fitting their I and I^* profiles from HI photolysis using Processes (12) through (15) with $k_{12} = 1.5 \times 10^{-13}$ and $k_{14} = 5 \times 10^{-11}$ cm^3/molecule-sec, respectively. In other experiments,[41] qualitatively similar fast initial decays of I^* (and fast formation of I) are followed by a slower decay at long times. Our data at high degrees of photolysis are qualitatively similar, but appear to differ quantitatively from those of Ref. 40. We do not discuss our non-single-exponential data in this study. By reducing the laser photolysis flux and increasing the signal averaging period, we were able to observe

single exponential decays over a wide range of $[HI]_0$. These data, plotted in Fig. 5, yield a rate coefficient $k_{12} = (5.7 \pm 1.0) \times 10^{-14}$ cm^3/molecule-sec. Previous results cluster around the values 5×10^{-14} and 1.5×10^{-13} cm^3/molecule-sec (Table IV). The smaller value appears to be strongly favored by three recent studies including the present one. Thus, the analysis of the complex I^* traces in Ref. 40 must be seriously re-evaluated.

C. CO-PHOTOLYSIS OF O_2^* AND HI AT λ = 249 nm

In principle, the results presented in previous sections can be combined with other fundamental kinetic data on the oxygen-iodine laser to predict the performance of a laser based on photoinitiated O_2^*/HI mixtures. Recent work by Young and Houston[44] on laser dissociation of iodides to produce I^* in the presence of ground state O_2 has demonstrated that many of the iodine donors have complicated side reactions that affect the decay of the equilibrium in Eq. (3). Interestingly, HI and CH_3I were the only well-behaved I atom precursors studied. In a system containing only HI and O_2 (in its three lowest electronic states), many deleterious side reactions are possible; these are considered in this section.

$O_2(^3\Sigma)$ has an extremely weak absorption coefficient at 249 nm.[21] There are no known transitions originating from $O_2(^1\Delta)$ in this spectral region.[45,46] Experimentally, we have observed a minute amount of $O_2(^1\Sigma)$ when O_2 is irradiated at 249 nm. No change in that signal is observed when 5 to 10% of the O_2 is excited to $O_2(^1\Delta)$ by the microwave discharge. In the mixed O_2^*/HI system, O_2^* is capable of pumping $I(^2P_{3/2})$ to I^*. Therefore, we must explicitly account for Reaction (13) relative to other H atom sinks in determining the total density of I atoms in the system while recognizing that Process (3) controls the I^*/I distribution.

The H atoms formed by the photolysis of HI can also interact with the O_2 molecules in the system. The reaction[47]

$$H + O_2(^3\Sigma) \xrightarrow{k_{16}} OH + O(^3P) \qquad (16)$$

$$k_{16} = 3.7 \times 10^{-10} \exp(-16800/RT)$$

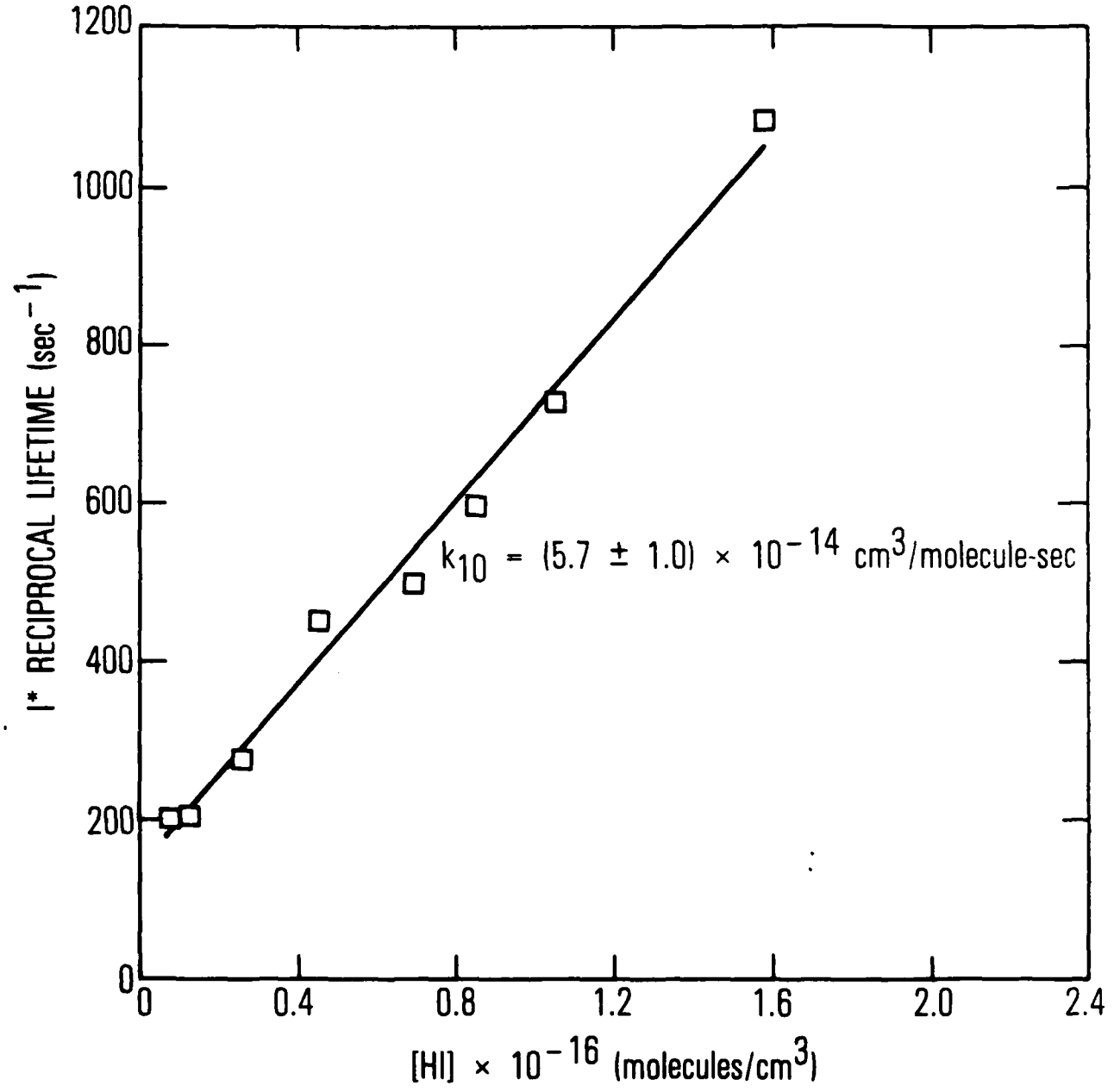

Fig. 5. First-order decay rates of I^* versus [HI]. Estimated percentage photolysis is 0.01%.

Table IV. Summary of Rate Coefficient Measurements

Process	Rate Coefficient (cm^3/molecule-sec)	Reference
$O_2(^1\Delta) + HI \rightarrow O_2(^3\Sigma) + HI$	$<2 \times 10^{17}$	This Work[a]
$O_2(^1\Sigma) + HI \rightarrow O_2(^1\Delta, ^3\Sigma) + HI$	$(2.5\pm1.0) \times 10^{-14}$	This Work[a]
	$(2.9\pm0.5) \times 10^{-14}$	This Work[b]
$I^* + HI \rightarrow I + HI$	$(5.7\pm1.0) \times 10^{-14}$	This Work[b]
	$(1.5\pm0.2) \times 10^{-13}$	40
	$(1.3\pm0.2) \times 10^{-13}$	41
	$(5.2\pm0.4) \times 10^{-14}$	42
	$(5 \pm 1) \times 10^{-14}$	43

[a]Measured by kinetic flow tube experiment.
[b]Measured by excimer laser photolysis experiment.

is endothermic by 17 kcal/mol and is, therefore, extremely slow at room temperature. As noted previously, however, the H atoms from the HI photolysis contain substantial translation energy,[22,23] having roughly 22 and 44 kcal/mol from Processes (9a) and (9b), respectively. Classical trajectory calculations for Process (16) have been performed on the lowest HO_2 potential energy surface at collision energies of 28, 60, and 90 kcal/mol.[48] An experimental total collision cross section of 0.42 $Å^2$ has been reported in a companion study[49] at 60 kcal/mol collision energy. Thermalization of the H atoms by T → T transfer with O_2 is rather inefficient; however, a recent study has indicated substantial vibrational (T → V) and rotational (T → R) excitation occurs in hot H atom collisions with diatomic partners.[50] Electronic excitation of O_2 by H is energetically feasible as well. Thus, translational cooling of H atoms is quite complex, yet it is vital to the suppression of both Reaction (16) and (17) relative to Reaction (13).

$$H + O_2(^1\Delta) \xrightarrow{k_{17a}} H + O_2(^3\Sigma) \qquad (17a)$$

$$\xrightarrow{k_{17b}} OH + O(^3P) \qquad (17b)$$

Glass and coworkers[51] have made a careful study of the temperature dependence of this process. Their rate coefficient of $k_{17} = (1.46 \pm 0.49) \times 10^{-11}$ $\exp(-4000 \pm 200$ cal-mol^{-1}/RT) cm^3/molecule-sec indicates that this process could be significant in a system where the H atoms are not thermalized. In addition, these authors favor Process (17b) over (17a) to explain their data, thus creating the possibility that OH and H_2O could be introduced into the present system, which has no diluent other than O_2 and O_2^*.

Figure 6 shows I^* decay traces for HI photolysis in Ar and HI photolysis in O_2/O_2^*. The only change in experimental conditions is the direct replacement of Ar by O_2/O_2^* (Table V). Curve (a) has a t = 0 amplitude determined by the HI quantum yield $[I^*/(I + I^*) = 0.65]$. Curve (b) has a t = 0 amplitude fixed by Process (3) $\{[I^*]/[I] = (k_3/k_{-3}) \times [O_2(^1\Delta)]/[O_2(^3\Sigma)]\}$. Calculated and measured ratios are presented in Table V. We find that the measured I^*/I

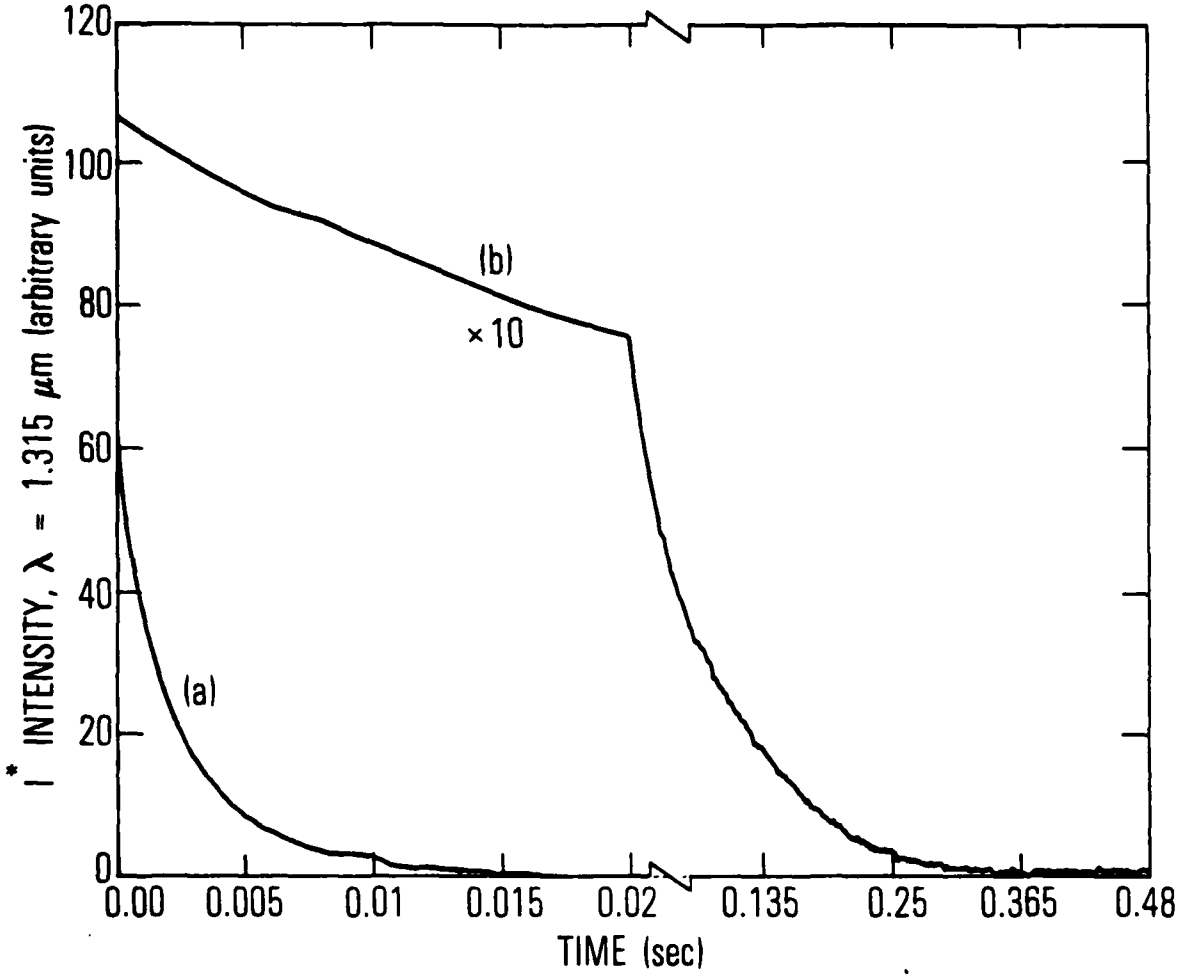

Fig. 6. I^* decay profiles from HI photolysis.
Curve (a): $[Ar] = 1.0 \times 10^{17}$, $[HI]_0 = 2.8 \times 10^{15}/cm^3$.
Curve (b): $[O_2(^3\Sigma)] = 9.1 \times 10^{16}$, $[O_2(^1\Delta)] = 7.9 \times 10^{15}$, $[HI]_0 = 2.5 \times 10^{15}/cm^3$.

Table V. Photolysis of HI in Ar and in O_2^* at λ = 248.5 nm

Run	[Ar] ($\times 10^{17}$)	[$O_2(^3\Sigma)$] ($\times 10^{17}$)	[$O_2(^1\Delta)$] ($\times 10^{15}$)	HI ($\times 10^{15}$)	R_1[a]	R_2[b]	R_3[c]
1	1.0	0	0	0.81	0.65	-	-
2	0	0.90	7.9	0.65	-	0.20	0.20
3	1.0	0	0	2.8	0.65	-	-
4	0	0.91	7.9	2.5	-	0.20	0.12
5	1.0	0	0	4.8	0.65	-	-
6	0	0.91	7.9	4.4	-	0.20	0.10

[a] $R_1=[I^*]/([I^*]+[I])$ based on photolysis quantum yield data.

[b] $R_2=[I^*]/([I^*]+[I])$ is calculated (see text) from the measured $O_2(^1\Delta)/O_2(^3\Sigma)$ ratio prior to HI injection.

[c] $R_3=[I^*]/([I^*]+[I])$ is based on comparing the t = 0 I^* signal from HI photolysis in O_2^* to that from HI photolyzed in Ar.

ratios are somewhat smaller than the calculated ratios, implying that the added HI, added I_2 impurity, or the photolysis process causes some quenching of $O_2(^1\Delta)$. It is obvious that the time scale of the I^* decay is significantly lengthened in the presence of $O_2(^1\Delta)$ (Fig. 6b). In fact, the effect is even more pronounced than Fig. 6b indicates. We must analyze this long time decay in detail in order to establish the amount of H_2O that has been generated by the photolysis of HI in O_2^*/O_2.

We have found that the main limitation on the I^*/O_2^* decay at long times is often not gas-phase quenching, but rather the time required to pump the laser-excited cylinder of gas (Fig. 1) past the observation window. Figure 7a shows a simulation of this process achieved by terminating the microwave discharge and measuring the time response of $O_2(^1\Sigma)$, which is in steady state with $O_2(^1\Delta)$. The axial diffusion problem which is superimposed on this cell pumpout time can be solved analytically[52] to give the following expression:

$$[O_2(^1\Sigma)] = 1/2[O_2(^1\Sigma)]_0[1 + f(z)] \qquad (18)$$

where f is the Gaussian error integral, $z = x/[2(Dt)^{1/2}]$, D is the diffusion coefficient of O_2^* in O_2, and x is distance along the flow tube axis. It is then convenient to define the quantity $w_d = 2(Dt)^{1/2}$ which represents the distance between 0.25 and 0.75 $[O_2(^1\Sigma)]_0$. In this experiment, distance is converted to time by dividing by the plug flow velocity in order to calculate the time response at a fixed downstream observation point. The data in Fig. 7a [curve (a)] can be fit precisely by Eq. (18), which describes the effect of axial diffusion on the bulk transport of the O_2^* out of the cell.

If the laser photolysis zone does not fill the cell volume, one must account for radial diffusion as well. Ordinarily, the boundary condition for an excited state at a wall would be $[c^*] = 0$. In the present experiment, $O_2(^1\Delta)$ causes the $[I^*]$ to attain an average value as I atoms become uniformly distributed in the cell volume. As discussed previously,[8,9] $O_2(^1\Delta)$ is capable of dissociating any I_2 formed by I atom recombination on the walls, thus holding the total I atom concentration constant.

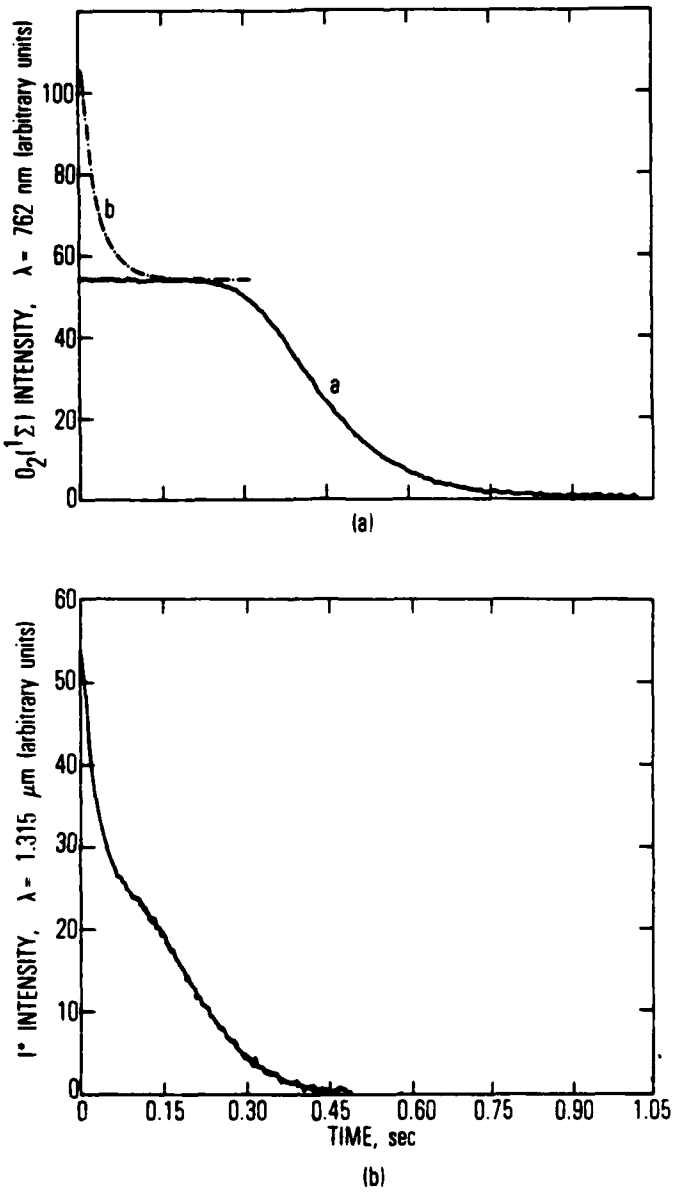

Fig. 7. Diffusion and flow limits on kinetic time scales.
(a) —— experimental pumpout/axial diffusion curve for $O_2(^1\Sigma)$ [curve (a)]. -.-.- postulated I^* radial diffusion curve for HI photolysis in O_2^* from photolysis volume to cell volume [curve (b)].

(b) Experimental I^* decay in O_2^* at low [HI]. $[O_2(^3\Sigma)] = 9.0 \times 10^{16}$, $[O_2(^1\Delta)] = 7.9 \times 10^{15}$, $[HI]_0 = 6.4 \times 10^{14}/cm^3$. Calculated percentage photolysis: 2.2%.

In addition to the measured axial diffusion curve, Fig. 7a [curve (b)] shows a calculated decay of $[I^*]$ for an inverse radial diffusion time of $\tau^{-1} = 30\ sec^{-1}$. This value was calculated from the radial diffusion equation in a long cylinder, where $\tau^{-1} = \{D_{12}[(\pi^2/L^2) + (5.81/R^2)]\}$.[53] D_{12} is taken to be the diffusion coefficient of Xe in Ar (0.10 cm^2/sec). The change in amplitude of this curve reflects the degree to which the detector collection optics favors collection of radiation from the laser photolysis volume as opposed to the total cell volume. In reality, the $O_2(^1\Delta)/I^*$ system would decay slowly from the plateau in Fig. 7a [curve (b)] even in the absence of axial diffusion effects due to slow gas phase and wall quenching. This behavior was ignored in these semi-quantitative arguments, but will be considered in Section IV.

The convolution of these diffusion effects can be expected to produce rather unusual decay curves at low HI densities where gas phase quenching processes are small. Figure 7b shows such a trace for I^*. Although we are monitoring I^*, the axial diffusion of O_2^* is an important parameter, because $O_2(^1\Delta)$ determines the $[I^*]$ in steady state as soon as radial diffusion homogeneously fills the cell with I atoms. Quantitatively similar results were obtained for $O_2(^1\Sigma)$, which is in steady state with I^* because of Process (4a). Figure 8 shows that the initial decay time of I^* is hardly altered by the photolysis of increasingly large amounts of HI. The detailed discussion of this behavior is presented in Section IV.

As we observed in time-resolved flow tube measurements on the O_2^*-I_2 system,[12] the behavior of $O_2(^1\Sigma)$ is perturbed by the creation of I^* as a consequence of the large rate coefficient for the pooling process, k_{4a}. The density of $^1\Sigma$ approaches steady state with a rate determined by the $^1\Sigma$ quenching process and decays with a rate determined by the quenching rate of $O_2(^1\Delta)$ [see Eq. (7)]. Under a wide range of conditions, the behavior of $O_2(^1\Sigma)$ mimics the time-behavior of I^*. Figure 9 demonstrates that such $O_2(^1\Sigma)$ behavior can be achieved in the excimer laser photolysis experiments. The complex long-time behavior is again in evidence. Contributions to $O_2(^1\Sigma)$ quenching were discussed in the context of Eqs. (6) through (8). The quenching rate can be defined[12] as

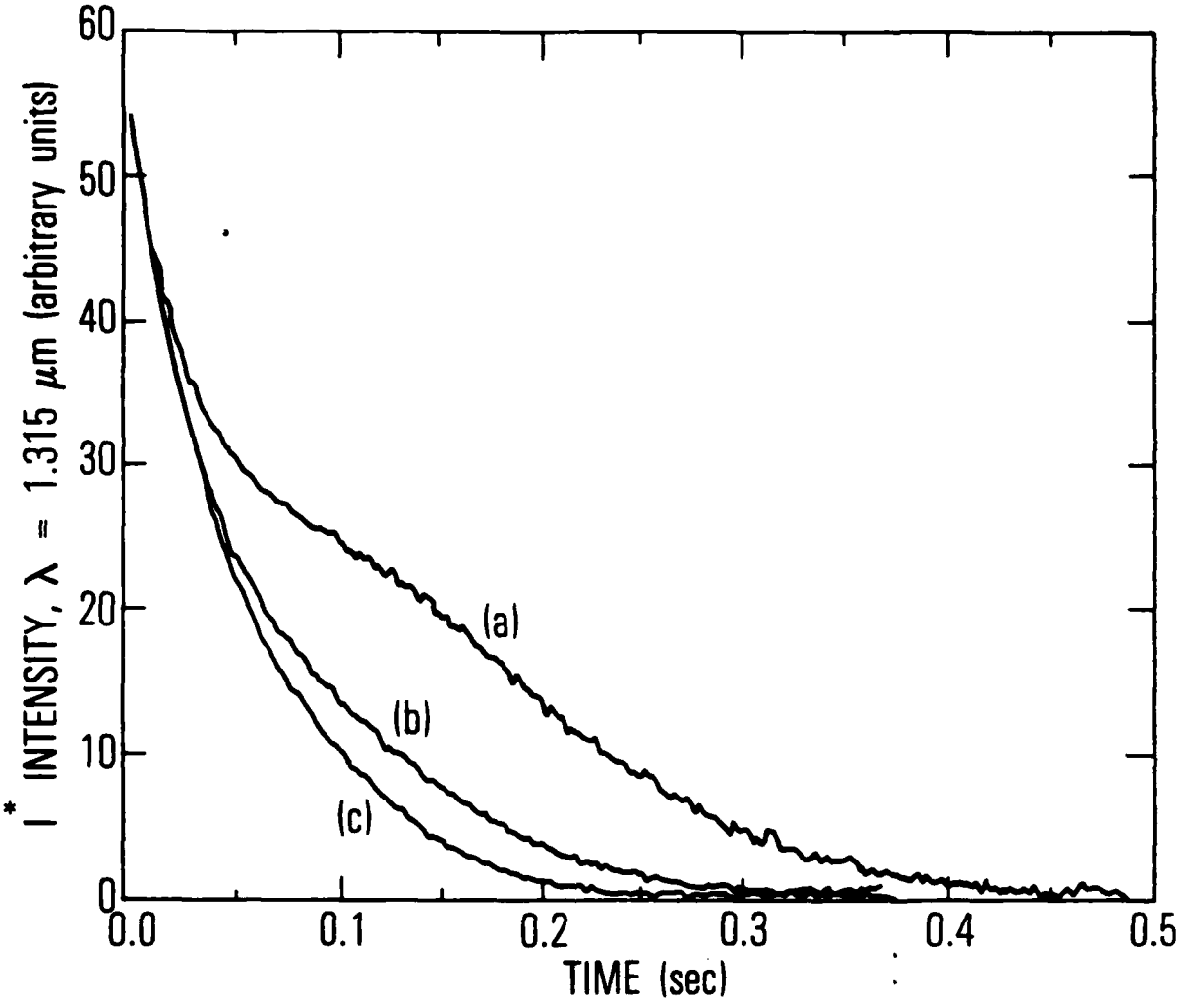

Fig. 8. Normalized I^* decay curves in O_2^* at low $[HI]_0$. $[O_2(^3\Sigma)] = 9.0 \times 10^{16}$, $[O_2(^1\Delta)] = 7.9 \times 10^{15}/cm^3$. Percentage photolysis: 2.2%. (a) $[HI]_0 = 6.4 \times 10^{14}$, (b), 2.5×10^{15}, (c) $4.4 \times 10^{15}/cm^3$.

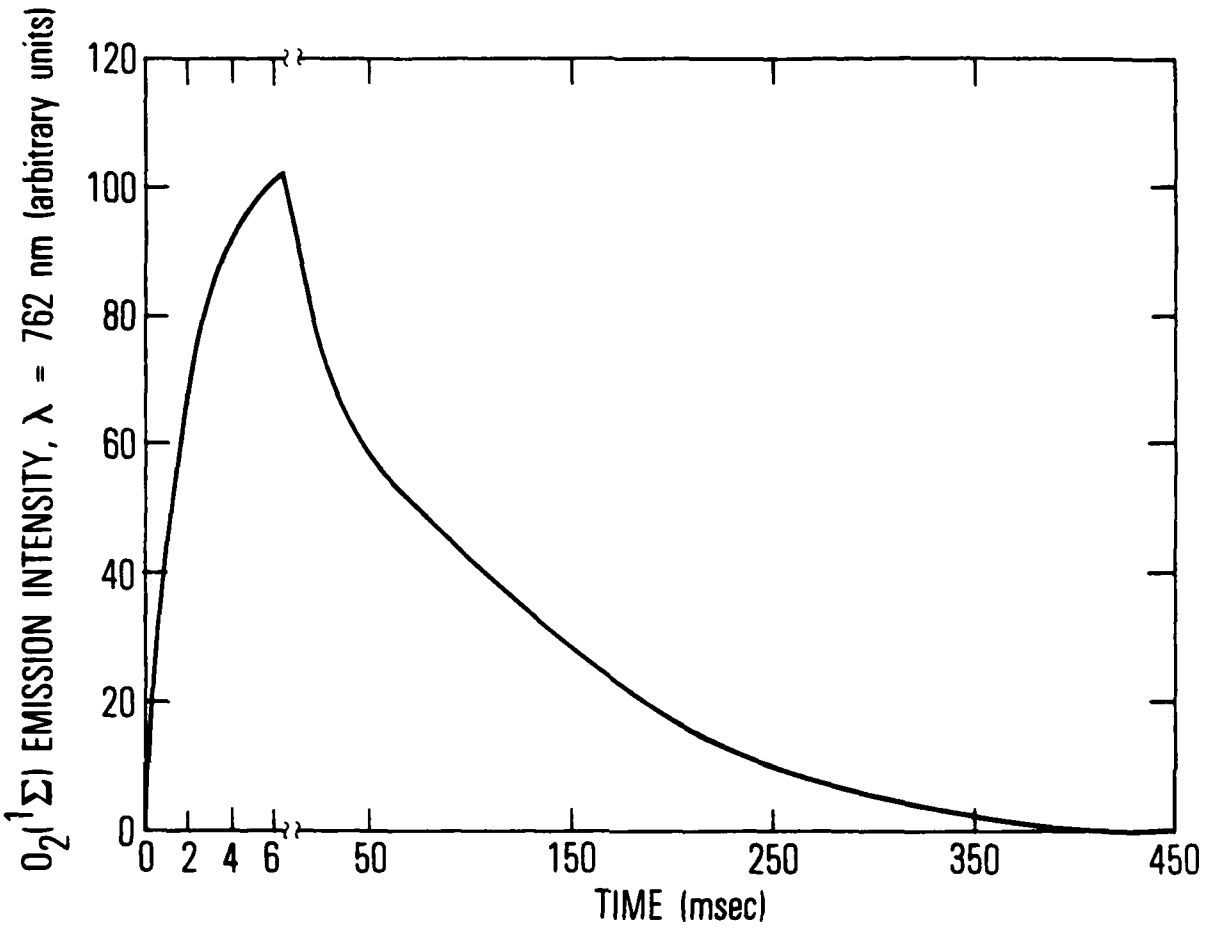

Fig. 9. Production and decay of $O_2(^1\Sigma)$ following HI photolysis in O_2*.

$$k_\Sigma = k_\Sigma^0 + k_6[HI] \qquad (19)$$

The inverse risetimes, τ_r^{-1}, are plotted in Fig. 10 versus $[HI]_0$ for constant fractional HI dissociation, f. From the photolysis fraction (f = 0.017) and the slope of the line in Fig. 10, we calculate $k_6 = 2.9 \times 10^{-14}$ cm^3/ molecule-sec in excellent agreement with the flow-tube study of Section III.A. Table IV summarizes the kinetic rate coefficients determined by the present investigation.

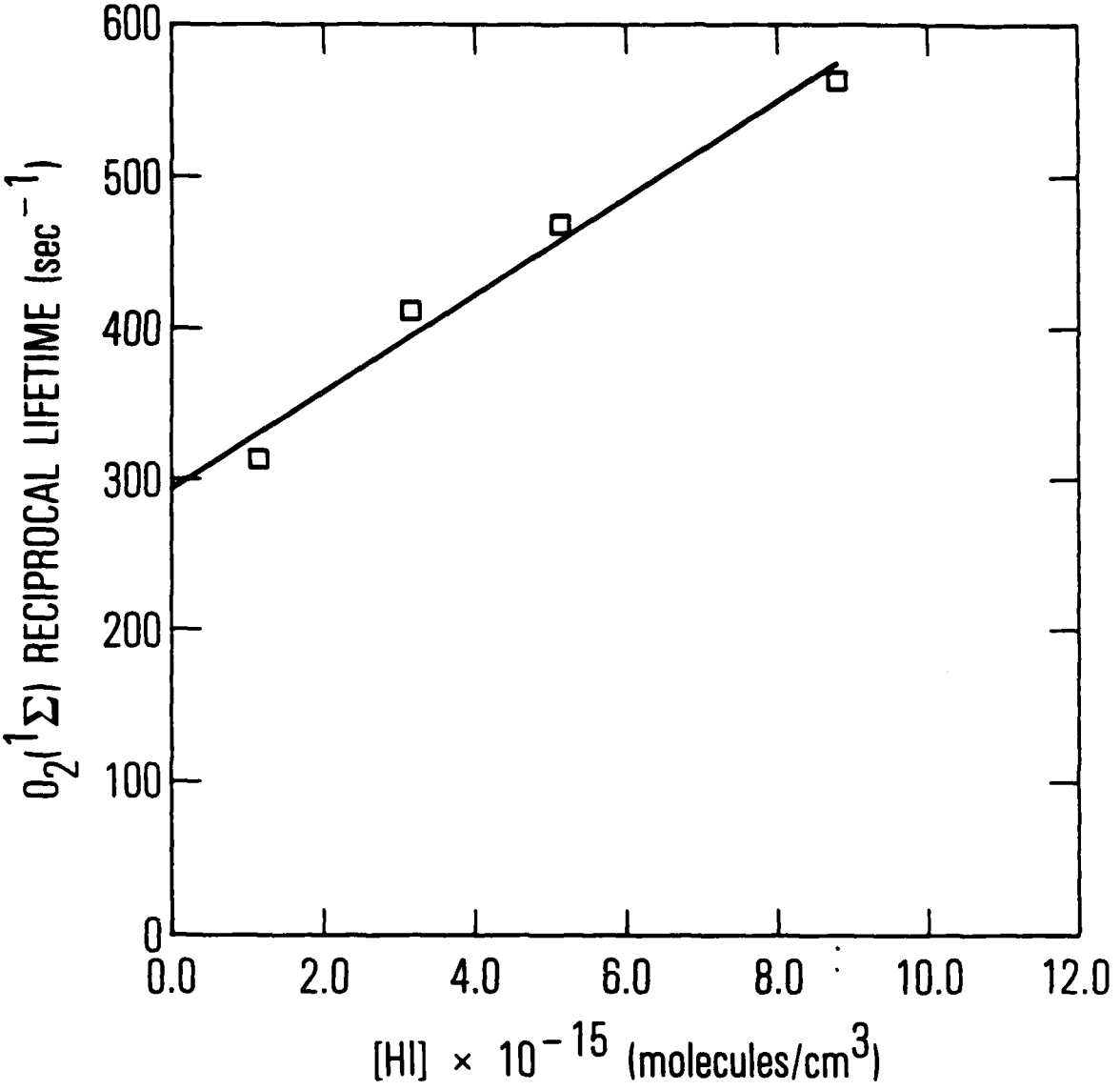

Fig. 10. Quenching rates (sec^{-1}) of $O_2(^1\Sigma)$ versus $[HI]_0$.

IV. DISCUSSION

Young and Houston[44] found that only two of the tested I^* atom precursors, HI and CH_3I, gave slow decays of the O_2^*-I^* equilibrium [Process (3)] at long decay times. Although CH_3I was not tested in the present study, it is apparently stable in discharged O_2. O'Brien and Myers[19] quote a rate coefficient for $O_2(^1\Sigma)$ quenching by CH_3I similar to the present measurement for Process (6). Based on the limited available data, I_2 and the perfluoroalkyl iodides appear to be unstable or reactive in O_2^*, whereas HI and at least some of the alkyl iodides are stable.

Given the small rate coefficients for Processes (1) ($< 2 \times 10^{-17}$ cm^3/molecule-sec) and (5) [$(2 \pm 1) \times 10^{-17}$ cm^3/molecule-sec][9,54,55], the decay of stored energy in $O_2(^1\Delta)$ is catalyzed by the presence of I atoms. The following processes were considered in addition to those previously specified:

$$O_2(^1\Delta) + I \xrightarrow{k_{20}} O_2(^3\Sigma) + I \qquad (20)$$

$$O_2(^1\Delta) + \text{wall} \xrightarrow{k_{21}} O_2(^3\Sigma) + \text{wall} \qquad (21)$$

$$I^* + O_2(^3\Sigma) \xrightarrow{k_{22}} I + O_2(^3\Sigma) \qquad (22)$$

$$I^* + Q_i \xrightarrow{k_{23}} I + Q_i \qquad (23)$$

$$I^* + \text{wall} \xrightarrow{k_{24}} I + \text{wall} \qquad (24)$$

where Q_i are the gas phase quenchers of I^*. An analytic expression can be derived leading to a predicted combined first- and second-order decay of $O_2(^1\Delta)$.[18] This expression is an extension of published work by Derwent and Thrush.[16]

$$\frac{1}{[O_2(^1\Delta)]} = \left\{ \frac{1}{[O_2(^1\Delta)]_0} + \frac{A}{B} \right\} \exp(Bt) - \left(\frac{A}{B}\right) \qquad (25)$$

where

$$A = k_5 + k_4[I^*]/[O_2(^1\Delta)]$$

and

$$B = \left\{\frac{k_{22}k_3}{(k_{22} + k_{-3})} + k_{20}\right\} [I] + k_{21} + \frac{[I^*]}{[^1\Delta]} \left\{k_{231}[Q_1] + k_{24}\right\}$$

$$= k_{eff}[I] + k_{21} + \frac{[I^*]}{[O_2(^1\Delta)]} \left\{k_{231}[Q_1] + k_{24}\right\}$$

The second-order quenching terms for $O_2(^1\Delta)$, Processes (4) and (5), are intrinsic to any oxygen-iodine laser. The first-order $O_2(^1\Delta)$ quenching terms, $k_{eff}[I] + k_{21}$, are relatively small.[18,54] Quenching of I^* is the main factor that degrades laser performance in any particular COIL device. That degradation becomes more severe as $I^*/O_2(^1\Delta)$ increases. This analysis was demonstrated on an O_2*-I_2-H_2O system in a previous report.[13]

The study by Pirkle et al.[15] employed densities of $O_2(^1\Delta)$, $O_2(^3\Sigma)$, and HI similar to those presented in Fig. 2. In that study, however, $O(^3P)$ atoms were not removed from the discharged O_2, and I atoms were generated by Reaction (2). Unfortunately, the initial $O(^3P)$ density was not measured explicitly. If we assume that all of the O atoms were titrated by added HI and that Reaction (2) is followed by

$$OH + HI \xrightarrow{k_{26}} H_2O + I \qquad (26)$$

or

$$OH + OH \xrightarrow{k_{27}} H_2O + O \qquad (27)$$

we obtain the stoichiometry

$$O(^3P) + 2\ HI \xrightarrow{k_{28}} H_2O + 2\ I \qquad (28)$$

which will be used in the calculation below. Using the equilibrium constant for Process (3) (K_{eq} = 2.9 at T = 295 K), we are able to derive the $O_2(^1\Delta)/O_2(^3\Sigma)$ ratio (0.06-0.11) from the reported $I^*/(I^* + I)$ ratios of 0.15-0.25. From the data in Ref. 15 (Fig. 4) we are able to calculate $I^*/O_2(^1\Delta)$ = 0.25 and to calculate a quenching coefficient for I^* by H_2O from those data

$$I^* + H_2O \overset{k_{29}}{\rightarrow} I + H_2O \tag{29}$$

$$\tau_{obs}^{-1} = k_{29}\,[H_2O]\,[I^*]/[O_2(^1\Delta)] \tag{30}$$

A value of $k_{29} = 2.7 \times 10^{-12}$ cm^3/molecule-sec is obtained from this analysis of the data in Ref. 15 in excellent agreement with values obtained by more direct methods.[56,57] Although data such as these are understandable in the context of the current model, it is clear that H_2O is an undesirable quencher in an oxygen-iodine laser.

Figure 8 shows that the initial decay (radial diffusion) time is hardly altered by the photolysis of $[HI]_0 = 4.4 \times 10^{15}/cm^3$ producing $([I] + [I^*])_0 = 1.9 \times 10^{14}/cm^3$. If we analyze curves (a), (b), and (c) in Fig. 8 at $t > 0.15$ sec, we estimate an enhancement of the $I^*/O_2(^1\Delta)$ removal rate of ~ 10 sec^{-1}. This is consistent with an enhancement due to Process (4) which is a second order process with an inverse half-life of 8.0 sec^{-1} for curve (c), and Process (12), which is a first-order process with an inverse lifetime defined by $[I^*]/[O_2(^1\Delta)] \times k_6[HI] = 1.0$ sec^{-1}.

If we ignore this calculation and assume that all the H atoms from Process (9) react by means of the reaction sequence (16), (26), and (2), we would observe the stoichiometry

$$H + O_2 + 3\,HI \rightarrow 2\,H_2O + 3\,I \tag{31}$$

This analysis creates several problems. First, the quantum yield of I atoms from such a sequence would be 4 instead of 2. This would cause the observed $I^*/(I^* + I)$ ratios reported in column R_3 of Table IV to exceed the correlation in column R_2. The opposite behavior is observed. Secondly, the concentration

of H_2O that would account for the entire 10 sec^{-1} rate acceleration is $1.4 \times 10^{14}/cm^3$ or roughly 50% of the maximum amount allowed by Eq. (31). We re-emphasize that the observed acceleration of the O_2^*/I^* decay can be accounted for by known rate processes other than H_2O quenching of I^*.

A more stringent test for H_2O production is the effect of H_2O on $O_2(^1\Sigma)$

$$O_2(^1\Sigma) + H_2O \overset{k_{32}}{\not\rightarrow} O_2(^1\Delta) + H_2O \qquad (32)$$

$$k_{32} = (5 \pm 2) \times 10^{-12}\ cm^3/molecule\text{-}sec^{58,59}$$

The data in Fig. 10 show that for 2% photolysis of $[HI]_0 = 1 \times 10^{16}/cm^3$ ($[H_2O]_{max} = 4 \times 10^{14}/cm^3$) that the $O_2(^1\Sigma)$ removal rate increases by $< 300\ sec^{-1}$. Of that increase $> 200\ sec^{-1}$ is accounted for by Process (6). This sets an upper limit on the amount of H_2O formed of $2 \times 10^{13}/cm^3$. In other words, < 5% of the H atoms [see Eq. (31)] produced by HI photolysis appear as H_2O and participate in $O_2(^1\Sigma)$ deactivation.

This discussion completes the assessment of HI as a premixed I-atom precursor for a pulsed COIL device. The main advantages of HI may be summarized as follows:

1. HI is an extremely inefficient quencher of $O_2(^1\Delta)$. This permits these two species to be uniformly mixed priof to photoinitiation.

2. The photolysis of HI in O_2/O_2^* has been found to create low densities of I^* quenchers, thus permitting high excited state densities to be consistent with long inversion times.

V. CONCLUSIONS

The molecule HI has been shown to be a suitable precursor for I atoms in a premixed O_2^*-I atom transfer laser that uses photolytic initiation. Other initiation methods or I atom precursors may be feasible. Although the quantum yield of I^* is quite high (65%) for monochromatic HI photolysis at $\lambda = 249$ nm, the I^* behavior is dominated by energy transfer from $O_2(^1\Delta)$. At the HI densities ($< 1 \times 10^{16}/cm^3$) and photolysis fraction (< 2%) studied, the behavior of the system closely resembled the predictions of a simple kinetic model that incorporated the known kinetics of the chemical oxygen-iodine laser (COIL) and the kinetics of HI with O_2^* and I^* as reported in these experiments. Thus, the kinetics of H atoms with O_2^*/O_2 and subsequent reactions involving $O(^3P)$ and OH appear to play a minor role in this proposed pulsed chemical laser device.

REFERENCES

1. W. E. McDermott, N. R. Pchelkin, D. J. Benard, and R. R. Bousek, Appl. Phys. Lett. 32, 469 (1978).

2. D. J. Benard, W. E. McDermott, N. R. Pchelkin, and R. R. Bousek, Appl. Phys. Lett. 34, 40 (1979).

3. R. J. Richardson and C. E. Wiswall, Appl. Phys. Lett. 35, 138 (1979).

4. K. Hohla and K. L. Kompa, in Handbook of Chemical Lasers, edited by J. F. Bott and R. W. F. Gross (Wiley-Interscience, New York, 1976).

5. G. Brederlow, E. Fill, and K. J. Witte, The High Power Iodine Laser, Springer Series in Optical Sciences, Vol. 34 (Springer, New York, 1983).

6. G. N. Hays and G. A. Fisk, IEEE J. Quantum Electron. QE-17, 1823 (1981).

7. G. E. Busch, IEEE J. Quantum Electron. QE-17. 1128 (1981).

8. R. F. Heidner III, C. E. Gardner, G. I. Segal, and T. M. El-Sayed, J. Phys. Chem. 87, 2348 (1983).

9. H. V. Lilenfeld, Oxygen-Iodine Laser Kinetics, AFWL-TR-83-01, McDonnell Douglas Research Laboratory, St. Louis, Mo., May, 1983.

10. R. F. Heidner III (unpublished results).

11. S. J. Davis and P. D. Whitefield (to be published).

12. R. F. Heidner III, C. E. Gardner, T. M. El-Sayed, G. I. Segal, and J. V. V. Kasper, J. Chem. Phys. 74, 5618 (1981).

13. R. F. Heidner III, C. E. Gardner, T. M. El-Sayed, and G. I. Segal, Chem. Phys. Lett. 81, 142 (1981).

14. D. W. Trainor, D. O. Ham, and F. Kaufman, J. Chem. Phys. 58, 4599 (1973).

15. R. J. Pirkle, J. R. Wiesenfeld, C. C. Davis, G. J. Wolga, and R. A. McFarlane, IEEE J. Quantum Electron. QE-11, 834 (1975).

16. R. G. Derwent and B. A. Thrush, Discuss. Faraday Soc. 53, 162 (1972).

17. H. V. Lilenfeld, P. A. G. Carr, and F. E. Hovis, Chem. Phys. Lett. 93, 38 (1982).

18. R. F. Heidner III (to be submitted for publication).

19. R. J. O'Brien and G. H. Myers, J. Chem. Phys. 53, 3832 (1970).

20. A. M. Pravilov, Sov. J. Quantum Electron. 11, 847 (1981).

21. J. G. Calvert and J. N. Pitts, Photochemistry (Wiley, New York, 1966), p. 180.

22. R. M. Martin and J. E. Willard, J. Chem. Phys. 40, 2999 (1964).

23. R. Schmiedl, H. Dugan, W. Meier, and K. H. Welge, Z. Phys. A. 304, 137 (1982).

24. R. S. Mulliken, Phys. Rev. 51, 310 (1937).

25. R. D. Clear, S. J. Riley, and K. R. Wilson, J. Chem. Phys. 63, 1340 (1975).

26. J. A. Betts, Ph.D. thesis, California Institute of Technology, 1971, available as #71-17375 from University Microfilms, Ann Arbor, MI.

27. T. Donohue and J. R. Wiesenfeld, Chem. Phys. Lett. 33, 176 (1975).

28. T. Donohue and J. R. Wiesenfeld, J. Chem. Phys. 63, 3130 (1975).

29. E. Gerck, Opt. Commun. 41, 102 (1982).

30. E. Gerck and E. Fill, Opt. Lett. 7, 25 (1982).

31. J. E. Smedley and S. R. Leone, J. Chem. Phys. 79, 2687 (1983).

32. H. Hofmann and S. R. Leone, J. Chem. Phys. 69, 3819 (1978).

33. J. B. Koffend and S. R. Leone, Chem. Phys. Lett. 81, 136 (1981).

34. V. S. Ivanov, A. S. Kozlov, A. M. Pravilov, and E. P. Smirnov, Sov. J. Quantum Electron. 10, 566 (1980).

35. J. F. Ogilvie, Trans. Faraday Soc. 67, 2205 (1971).

36. E. Gerck, J. Chem. Phys. 79, 311 (1983).

37. P. Cadman and J. C. Polanyi, J. Phys. Chem. 72, 3715 (1968).

38. D. R. Davis, J. M. White, J. Asay, and A. Kuppermann (private communication cited in Ref. 37).

39. J. H. Sullivan, J. Chem. Phys. 36, 1925 (1962).

40. T. Donohue and J. R. Wiesenfeld, J. Phys. Chem. 80, 437 (1976).

41. R. J. Donovan and D. Husain, Trans. Faraday Soc. 62, 1050 (1966).

42. R. J. Donovan, C. Fotakis, and M. F. Golde, J. C. S. Faraday II 72, 2055 (1976).

43. A. T. Pritt, Jr. and R. D. Coombe, J. Chem. Phys. 65, 2096 (1976).

44. A. T. Young and P. L. Houston, J. Chem. Phys. 78, 2317 (1983).

45. R. J. Collins, D. Husain, and R. J. Donovan, J. C. S. Faraday II 69, 145 (1973).

46. S. Ogawa and M. Ogawa, Can. J. Phys. 53, 1845 (1975).

47. D. L. Baulch, D. D. Drysdale, D. G. Horne, and A. C. Lloyd, Evaluated Kinetic Data for High Temperature Reactions, Vol. 1 (Butterworth, London, 1972), pp. 9-36.

48. K. Kleinermanns and R. Schinke, J. Chem. Phys. 80, 1440 (1984).

49. K. Kleinermanns and J. Wolfrum, J. Chem. Phys. 80, 1440 (1984).

50. S. R. Leone, XIth International Conference on Photochemistry, College Park, Md., 1983.

51. L. T. Cuppitt, G. A. Takacs, and G. P. Glass, Int. J. Chem. Kinet. 14, 487 (1982).

52. See, for example, the corresponding transient thermal analysis in W. H. McAdams, Heat Transmission (McGraw Hill, New York, 1954).

53. R. J. Donovan and D. Husain, Advances in Photochemistry 8, 1 (1971).

54. R. G. Derwent and B. A. Thrush, Trans. Faraday Soc. 67, 2036 (1971).

55. G. A. Fisk and G. N. Hays, J. Chem. Phys. 77, 4965 (1982).

56. D. H. Burde and R. A. McFarlane, J. Chem. Phys. 64, 1850 (1976).

57. A. J. Grimley and P. L. Houston, J. Chem. Phys. 69, 2339 (1978).

58. R. G. O. Thomas and B. A. Thrush, J. Chem. Soc. Faraday II 71, 664 (1975).

59. R. G. Aviles, D. F. Muller, and P. L. Houston, Appl. Phys. Lett. 37, 358 (1980), and references therein.

LABORATORY OPERATIONS

The Laboratory Operations of The Aerospace Corporation is conducting experimental and theoretical investigations necessary for the evaluation and application of scientific advances to new military space systems. Versatility and flexibility have been developed to a high degree by the laboratory personnel in dealing with the many problems encountered in the nation's rapidly developing space systems. Expertise in the latest scientific developments is vital to the accomplishment of tasks related to these problems. The laboratories that contribute to this research are:

Aerophysics Laboratory: Launch vehicle and reentry aerodynamics and heat transfer, propulsion chemistry and fluid mechanics, structural mechanics, flight dynamics; high-temperature thermomechanics, gas kinetics and radiation; research in environmental chemistry and contamination; cw and pulsed chemical laser development including chemical kinetics, spectroscopy, optical resonators and beam pointing, atmospheric propagation, laser effects and countermeasures.

Chemistry and Physics Laboratory: Atmospheric chemical reactions, atmospheric optics, light scattering, state-specific chemical reactions and radiation transport in rocket plumes, applied laser spectroscopy, laser chemistry, battery electrochemistry, space vacuum and radiation effects on materials, lubrication and surface phenomena, thermionic emission, photosensitive materials and detectors, atomic frequency standards, and bioenvironmental research and monitoring.

Electronics Research Laboratory: Microelectronics, GaAs low-noise and power devices, semiconductor lasers, electromagnetic and optical propagation phenomena, quantum electronics, laser communications, lidar, and electro-optics; communication sciences, applied electronics, semiconductor crystal and device physics, radiometric imaging; millimeter-wave and microwave technology.

Information Sciences Research Office: Program verification, program translation, performance-sensitive system design, distributed architectures for spaceborne computers, fault-tolerant computer systems, artificial intelligence, and microelectronics applications.

Materials Sciences Laboratory: Development of new materials: metal matrix composites, polymers, and new forms of carbon; component failure analysis and reliability; fracture mechanics and stress corrosion; evaluation of materials in space environment; materials performance in space transportation systems; analysis of systems vulnerability and survivability in enemy-induced environments.

Space Sciences Laboratory: Atmospheric and ionospheric physics, radiation from the atmosphere, density and composition of the upper atmosphere, aurorae and airglow; magnetospheric physics, cosmic rays, generation and propagation of plasma waves in the magnetosphere; solar physics, infrared astronomy; the effects of nuclear explosions, magnetic storms, and solar activity on the earth's atmosphere, ionosphere, and magnetosphere; the effects of optical, electromagnetic, and particulate radiations in space on space systems.

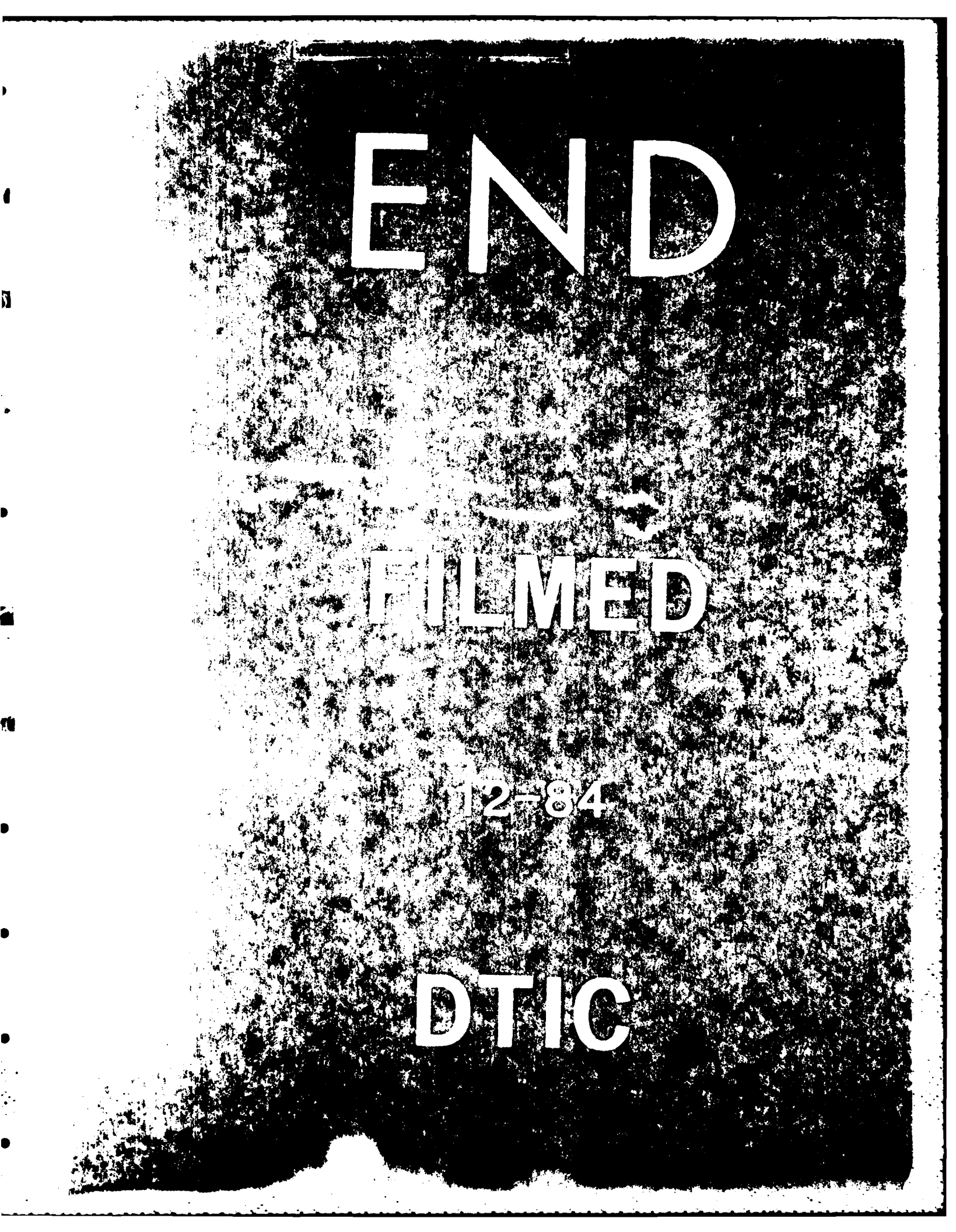
END
FILMED
12-84
DTIC